American Mineralogist, Volume 81, pages 1237–1248, 1996

Geochemical alteration of pyrochlore group minerals: Betafite subgroup

GREGORY R. LUMPKIN[1] AND RODNEY C. EWING[2]

[1]Materials Division, Australian Nuclear Science and Technology Organisation, Menai, New South Wales 2234, Australia
[2]Department of Earth and Planetary Sciences, University of New Mexico, Albuquerque, New Mexico 87131, U.S.A.

ABSTRACT

Relatively low-temperature, secondary alteration is common in samples of metamict betafite and initially proceeds by the substitution mechanisms $^{A}Na^{Y}F \rightarrow {}^{A}\square^{Y}\square$, $^{A}Ca^{Y}O \rightarrow {}^{A}\square^{Y}\square$, and $^{A}Ca^{X}O \rightarrow {}^{A}\square^{X}\square$. Alteration is usually accompanied by hydration (~10–15 wt% H_2O) together with minor increases in Al, K, Mn, Fe, Sr, and Ba. At this stage, U and Th remain relatively unaffected by the alteration process. Once Na and F are removed and the Ca content drops below about 0.2–0.3 atoms per formula unit (~2.5–3.5 wt% CaO), betafite bulk compositions fall within the stability field of liandratite + uranpyrochlore + rutile (or anatase), thus promoting major element mobility (including Th, U, Pb, and B-site cations), incipient recrystallization, and partial dehydration. New phase assemblages occur as a function of decreasing bulk U content in the order liandratite + rutile, liandratite + uranpyrochlore + rutile, and uranpyrochlore + rutile. The same phase assemblages also occur in laboratory heating experiments performed in an inert atmosphere at 1000 °C. Up to 20–30% of the original amount of U may be lost during severe secondary alteration and recrystallization of betafite. Part of this U is retained by liandratite crystallized in the adjacent host rock. Loss of radiogenic Pb results from both long-term diffusion and secondary alteration, aided by radiation damage-induced volume expansion and microfracturing.

INTRODUCTION

The betafite subgroup of the pyrochlore group is defined by $2Ti \geq Nb + Ta$ for the B-site cation population (Hogarth 1977). Individual species of the subgroup are found principally in carbonatite, calcite-fluorite-apatite-amphibole veins, and subalkaline to peralkaline anorogenic granitic pegmatites (Hogarth 1961; Kennedy 1979; Černý and Ercit 1989). Because of the general absence of modern chemical or electron microprobe analyses, only limited data are available regarding the general chemistry and geochemical alteration of betafite. Hogarth (1961) demonstrated that a compositional series exists between pyrochlore and betafite, thus firmly establishing betafite as a member of the pyrochlore group. Prior to the discovery of crystalline calciobetafite in a 0.084 Ma sanidinite from Italy (Mazzi and Munno 1983), betafite specimens were known to occur only in the metamict state. The compositions of most of these radiation-damaged betafite samples were notably deficient in Ca and contained little or no Na and F (Hogarth 1961, Table 2).

Most betafite samples described prior to 1980 approach the AB_2O_6 stoichiometry characteristic of many defect pyrochlores, with <0.6 Ca, 0.1 Na, and 0.1 F atoms per formula unit. Calciobetafite from the type locality approaches ideal $A_2B_2O_7$ stoichiometry with 1.3 Ca, 0.2 Na, and 0.3 F atoms per formula unit (Mazzi and Munno 1983). A study of alteration effects by Lumpkin and Ewing (1985) suggested that secondary alteration could be a major cause of nonstoichiometry in betafite. This was further demonstrated by Lumpkin et al. (1988) in a study of betafite from Madagascar. Patches of relatively unaltered material within the specimen were found to approach the composition $A_{1.7}B_2X_6Y_{1.7}$ with up to 0.8 Ca, 0.3 Na, and 0.2 atoms per formula unit (Lumpkin et al. 1988).

This study aims to provide a more complete description of alteration effects in members of the betafite subgroup and is the final paper in a series outlining the behavior of pyrochlore group minerals in the presence of hydrothermal and low-temperature fluids (Lumpkin and Ewing 1992, 1995). The results of this study are particularly relevant to the disposal of high-level nuclear waste with the use of crystalline ceramic materials, especially the titanate-based waste forms in which a pyrochlore phase is present in major amounts, serving as a major host for actinides (e.g., Harker 1988; Ringwood et al. 1988; Ball et al. 1989).

SAMPLE DESCRIPTION

A detailed description of the samples used in this study is given in Table 1. Except for the presence of secondary phases, all the betafite samples were rendered amorphous by natural α decay of ^{232}Th, ^{235}U, and ^{238}U incorporated at the A site, having received doses of $>3 \times 10^{17}$ α/mg

0003–004X/96/0910–1237$05.00

TABLE 1. Localities, sources, and associated minerals for nine betafite samples

No.	Locality	Alteration and mineral association	Source
081	Madagascar	0.5 cm crystal, turbid alteration, secondary Rut	USNM 96864
083	Silver Crater mine, Bancroft, Ontario, Canada	1.3 cm crystal, alteration along voids and microfractures, secondary galena, host rock: Cc + Bt + Ap ± Zrc	USNM 126235
155	Ambotofotsy, Madagascar	1 cm crystal, turbid alteration, sperulites, veinlets, secondary Hem + Eux + Rut, primary Ilm	SU 52559
176	Antanifotsy, Madagascar	1.6 cm crystal, turbid alteration, secondary Ldt	AMNH C81897
178	Felixtlahuaca, Oaxaca, Mexico	1.5 cm mass, unaltered(?), primary Cbt inclusions	AMNH 28426
186	Impilanti, Finland	1.4 cm mass, very dark, turbid alteration, secondary Goe	AMNH 17758
204	Silver Crater mine, Bancroft, Ontario, Canada	1 cm crystal, alteration along voids and microfractures, secondary galena, host rock: Cc + Bt + Ap ± Zrc	HU 124374
205	Antanifotsy, Madagascar	1.5 cm crystal, transparent core, turbid intermediate zone, recrystallized rim with secondary Rut + Ana + Ldt, host rock: Qtz + Ms + Kfs (altered to Kao)	HU 87876
210	Madagascar	2.2 cm crystal, transparent alteration, turbid alteration, secondary Ana	HU 81199

Note: Mineral abbreviations are as follows: Ana = anatase, Ap = apatite, Bt = biotite, Cbt = columbite, Cc = calcite, Eux = euxenite, Goe = goethite, Hem = hematite, Ilm = ilmenite, Kao = kaolinite, Kfs = potassium feldspar, Ldt = liandratite, Ms = muscovite, Qtz = quartz, Rut = rutile, and Zrc = zircon.

(Lumpkin and Ewing 1988). Primary alteration of the type commonly observed in microlite and pyrochlore (Lumpkin and Ewing 1992, 1995) was not found in any of the betafite samples examined in this study. The observed alteration of betafite is classified as secondary on the basis of the combination of fracture control and host-rock alteration in near-surface weathering environments. Alteration effects for samples from Madagascar are illustrated using optical photomicrographs in Figure 1. In sample 210, areas of unaltered betafite (yellow-orange) are surrounded by moderately altered (colorless) or highly altered (turbid) areas localized along microfractures (Fig. 1a). Incipient crystallinity is present within the turbid areas (Fig. 1b), identified by X-ray diffraction (XRD) as a mixture of anatase, pyrochlore, and liandratite (UNb_2O_8).

Sample 205, also from Madagascar, exhibits an unusual zonal alteration pattern and has a core similar in appearance to the colorless alteration of sample 210, an intermediate zone consisting of a mixture of colorless and dark turbid material with some microcrystalline spots, and a partially recrystallized rim (Figs. 1c–1f). Crystalline phases in the rim were identified by XRD as rutile, anatase, liandratite, and pyrochlore. Part of the host rock is preserved at the surface of the crystal and contains an assemblage of quartz, clay minerals, iron oxides, muscovite, and altered feldspars. Minor amounts of liandratite were identified in fractures extending for a short distance out into the host rock.

Additional betafite samples from Madagascar (081, 155, 176) and Finland (186) are completely altered to a material resembling the turbid areas of sample 210 and the intermediate zone of sample 205. Secondary electron images of sample 155 exhibit extremely fine-scale alteration (Figs. 2a and 2b), including areas with patchy contrast, fibrous material, U- and Ti-rich veinlets, and irregular patches and veinlets of euxenite and hematite. Crude spherulites were observed in some areas of the sample (Fig. 2a), a feature previously observed in metamict polycrase (Ewing 1974). Backscattered electron images show that alteration is also a common feature of betafite samples 083 and 204 from the Silver Crater mine near Bancroft, Ontario, Canada. The alteration is readily apparent as areas of low contrast localized along voids and microfractures, some of which contain precipitates of galena (Figs. 2c and 2d).

CHEMICAL EFFECTS OF ALTERATION

Experimental procedures used in this investigation can be found in Lumpkin and Ewing (1992). Representative electron microprobe analyses and structural formulas of six samples are given in Table 2. The complete data set

→

FIGURE 1. Optical micrograph pairs illustrating alteration of betafite from Madagascar. Photographs **a, c,** and **e** were taken in plane-polarized light and **b, d,** and **f** with crossed polarizers. (**a** and **b**) Sample 210 showing unaltered yellow-orange isotropic betafite surrounded by colorless, partially altered betafite and dark, highly altered material with incipient crystallinity. (**c** and **d**) Sample 205 showing colorless, partially altered isotropic core and highly altered intermediate zone consisting of a mixture of colorless areas and dark material with incipient crystallinity. (**e** and **f**) Intermediate zone and partially recrystallized rim of sample 205. Rutile (R) is black, uranpyrochlore (P) is colorless and isotropic, liandratite (L) is colorless and highly anisotropic, and residual metamict phase (M) is olive green and exhibits yellow-brown to bluish light scattering under crossed polarizers. Field of view in all photographs is 0.2 mm.

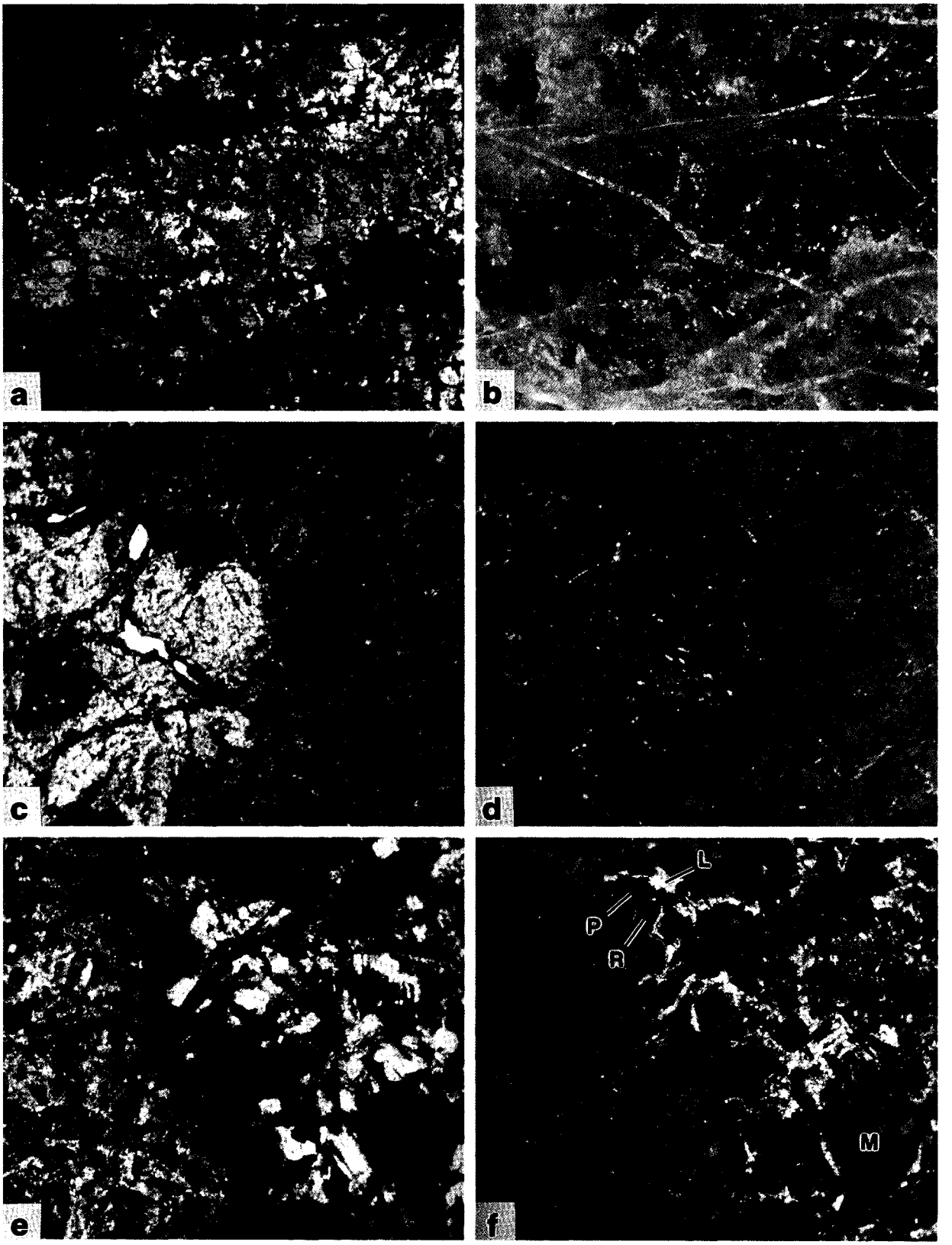
a
b
c
d
e
f
L
P
R
M

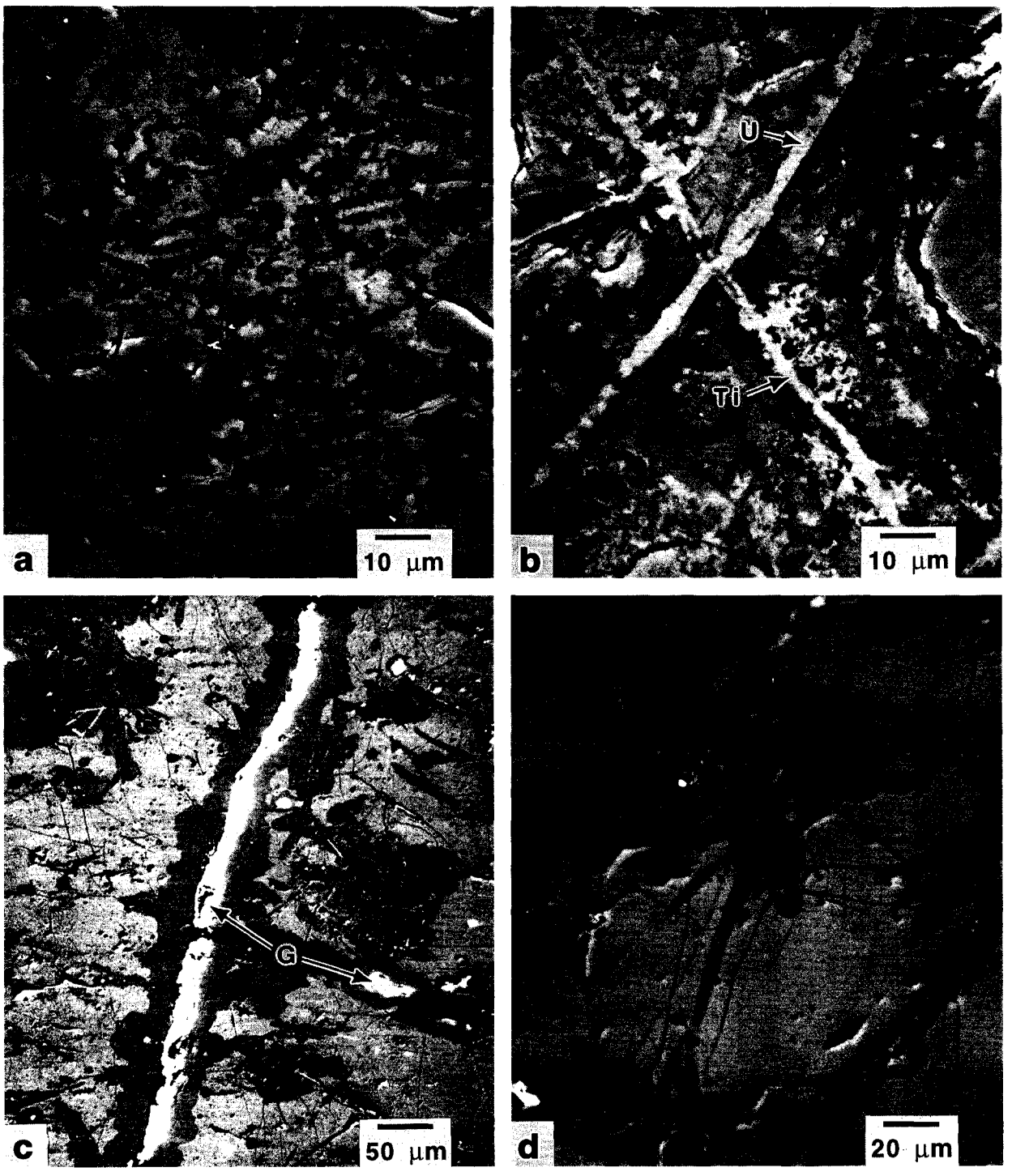

FIGURE 2. Scanning electron micrographs of altered betafite samples from Madagascar and Canada. (**a** and **b**) Secondary electron images showing details of stage 2 alteration in sample 155. Most areas of the sample (**a**) contain fibrous material and spherulites; a few areas (**b**) contain veinlets of Ti-rich material (Ti), U-rich material (U), euxenite, and hematite. (**c** and **d**) Backscattered electron images of sample 083 showing hydrated areas (dark gray) within relatively unaltered (light gray) betafite. Image **c** illustrates the common occurrence of galena (G) in microfractures and voids. Taken at higher magnification, image **d** shows how the alteration followed some of the fractures and voids. Many smaller voids were inaccessible, and some microfractures appear to postdate the alteration.

TABLE 2. Representative electron microprobe analyses of six betafite samples

	081s	081s	155s	155s	176s	176s	186s	186s	204	204s	210	210s
Nb_2O_5	25.4	26.9	35.2	27.8	34.2	28.2	22.3	25.0	36.1	34.4	32.9	35.3
Ta_2O_5	4.16	4.42	4.64	4.32	2.20	1.80	18.2	2.26	1.87	1.50	3.50	2.98
TiO_2	18.2	21.3	19.5	17.2	41.4	21.1	13.4	33.0	17.4	16.6	17.8	19.6
ZrO_2	0.02	0.00	0.02	0.00	0.00	0.03	0.22	0.11	0.09	0.00	0.00	0.07
ThO_2	1.32	1.56	2.53	2.07	1.21	0.53	0.93	0.51	0.41	0.29	1.88	1.91
UO_2	29.4	29.7	26.2	34.3	12.8	36.2	20.6	13.0	26.2	23.8	27.7	29.1
Al_2O_3	0.11	0.15	0.08	0.30	2.98	1.64	0.84	0.18	0.12	0.14	0.11	0.03
Y_2O_3	0.50	0.12	0.64	0.31	0.01	0.13	1.16	1.17	0.31	0.24	0.34	0.47
Ln_2O_3	1.1	0.80	1.8	1.2	0.38	0.40	0.74	0.30	0.96	0.79	0.40	0.86
MgO	0.05	0.06	0.04	0.01	0.00	0.00	0.08	0.05	0.07	0.07	0.00	0.04
CaO	1.81	1.57	0.01	0.18	0.09	0.33	4.18	1.03	8.29	6.94	10.7	1.14
MnO	0.05	0.04	0.01	0.01	0.00	0.01	0.90	0.76	0.40	0.58	0.91	0.09
FeO	1.94	2.56	0.70	0.56	0.81	0.49	0.16	14.9	3.15	3.43	0.58	0.31
SrO	0.00	0.00	0.00	0.00	0.00	0.00	0.23	0.00	0.00	0.03	0.00	0.00
BaO	0.27	0.27	0.48	0.95	0.41	0.83	0.30	0.23	0.08	0.07	0.11	0.24
PbO	2.10	2.29	2.39	0.68	1.72	1.87	3.06	1.44	0.46	0.48	1.76	1.71
Na_2O	0.00	0.00	0.00	0.05	0.00	0.01	0.03	0.06	0.06	0.06	1.49	0.00
K_2O	0.23	0.20	0.17	0.98	0.16	0.60	0.17	0.05	0.05	0.04	0.03	0.10
F	0.00	0.00	0.00	0.00	0.17	0.00	0.17	0.35	0.22	0.31	1.0	0.00
Sum	86.66	91.94	94.41	90.92	98.54	94.17	87.67	94.40	96.24	89.77	101.21	93.95
O ≡ F	−0.00	−0.00	−0.00	−0.00	−0.07	−0.00	−0.07	−0.15	−0.09	−0.13	−0.42	−0.00
Total	86.66	91.94	94.41	90.92	98.47	94.17	87.60	94.25	96.15	89.64	100.79	93.95
Structural formulas based on Σ B = 2.00												
Nb	0.868	0.823	0.996	0.930	0.609	0.821	0.769	0.611	1.084	1.087	1.014	1.010
Ta	0.086	0.081	0.079	0.087	0.024	0.032	0.378	0.033	0.034	0.029	0.065	0.051
Ti	1.036	1.084	0.918	0.957	1.228	1.022	0.769	1.342	0.870	0.873	0.913	0.934
Zr	0.001	0.000	0.001	0.000	0.000	0.001	0.008	0.003	0.003	0.000	0.000	0.002
Al	0.010	0.012	0.006	0.026	0.139	0.125	0.076	0.011	0.009	0.012	0.009	0.002
Th	0.023	0.024	0.036	0.035	0.011	0.008	0.016	0.006	0.006	0.005	0.029	0.028
U	0.495	0.447	0.365	0.565	0.112	0.519	0.350	0.156	0.388	0.370	0.420	0.410
Y	0.020	0.004	0.021	0.012	0.000	0.004	0.047	0.034	0.011	0.009	0.012	0.016
Ln	0.030	0.020	0.041	0.032	0.005	0.009	0.021	0.006	0.023	0.020	0.010	0.020
Mg	0.006	0.006	0.004	0.001	0.000	0.000	0.009	0.004	0.007	0.007	0.000	0.004
Ca	0.147	0.114	0.001	0.014	0.004	0.023	0.342	0.060	0.590	0.520	0.781	0.077
Mn	0.003	0.002	0.001	0.007	0.000	0.001	0.058	0.035	0.023	0.020	0.053	0.005
Fe	0.123	0.145	0.037	0.035	0.027	0.026	0.010	0.674	0.175	0.201	0.033	0.016
Sr	0.000	0.000	0.000	0.000	0.000	0.000	0.010	0.000	0.000	0.001	0.000	0.000
Ba	0.008	0.007	0.012	0.028	0.006	0.021	0.009	0.005	0.002	0.002	0.003	0.006
Pb	0.043	0.042	0.040	0.014	0.018	0.032	0.063	0.021	0.008	0.009	0.032	0.029
Na	0.000	0.000	0.000	0.007	0.000	0.001	0.004	0.006	0.008	0.008	0.197	0.000
K	0.022	0.017	0.014	0.093	0.008	0.049	0.017	0.003	0.004	0.004	0.003	0.008
Σ A	0.919	0.829	0.571	0.836	0.192	0.694	0.956	1.010	1.245	1.190	1.574	0.619
O	5.923	5.750	5.531	5.903	4.551	5.566	5.861	5.474	6.181	6.092	6.362	5.601
F	0.000	0.000	0.000	0.000	0.021	0.000	0.041	0.060	0.046	0.069	0.216	0.000
Σ (X + Y)	5.923	5.750	5.531	5.903	4.572	5.566	5.902	5.534	6.227	6.161	6.578	5.601

Note: An "s" in the sample number indicates secondary alteration. B-site cations are Nb, Ta, Ti, Zr, and Al. All Fe assumed to be Fe^{2+} and allocated to the A site. Si, Sb, Sn, Cs, W, and Bi are typically near or below detection limits and are not reported. Ln = lanthanides.

is available separately as Table 3.[1] Eighteen individual oxides plus the sum of nine lanthanide oxides (Ln_2O_3 = La, Ce, Pr, Nd, Sm, Gd, Dy, Er, Yb) are listed together with F for each analysis; W, Si, Sn, Sb, Bi, and Cs are generally near or below detection limits and are not reported. The degree of hydration is estimated by difference for each analysis with a precision of approximately ±2 wt%. These estimates are in reasonable agreement with thermogravimetric analysis of samples 083, 155, 178, 186, 204, and the core of 205. Total weight loss for this group of samples ranged from 9 to 13 wt% and occurred in three steps: 125–150 °C (2.0–8.0 wt%), 370–480 °C (2.8–7.5 wt%), and 620–750 °C (0.5–1.3 wt%). Infrared spectroscopy of sample 178 (and other samples of the pyrochlore subgroup) indicates that H_2O is the predominant hydrous species present (Lumpkin 1989).

Electron microprobe analyses of betafite samples 083 and 204 indicate that the observed alteration (Figs. 2c and 2d) mainly involves hydration with only a slight increase in the number of A-site vacancies. On the basis of analytical totals, the H_2O content varies from 3–5 wt% in relatively unaltered areas to 10–12 wt% in altered areas. The two samples are similar in composition and contain 0.57–0.66 Ca, 0.00–0.02 Na, and 0.00–0.11 F atoms per formula unit. Betafite sample 178 contains 0.39–0.53 Ca, <0.01 Na, 0.00–0.12 F, and 0.02–0.04 Ba atoms per formula unit and 10–12 wt% H_2O (by difference). The sample exhibits no obvious alteration when observed in thin section. However, all three samples may have experienced some secondary alteration as indicated by the low Ca content, general absence of Na and F, and overall level

[1] Table 3 may be ordered as Document AM-96-622 from the Business Office, Mineralogical Society of America, 1015 Eighteenth Street NW, Suite 601, Washington, DC 20036, U.S.A. Please remit $5.00 in advance for the microfiche.

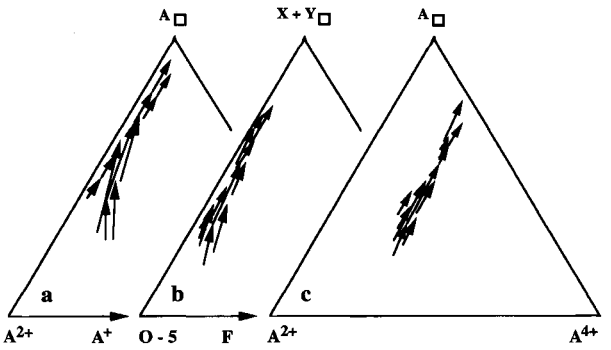

FIGURE 3. Triangular plots (atom ratios) showing stage 1 secondary alteration paths in metamict betafite (samples 083, 204, and 210). (a) Plot of A^{2+} cations (mainly Ca, Fe), A^{+} cations (mainly Na), and A-site vacancies. (b) Plot of O, F, and X + Y anion vacancies. O is plotted as O − 5 because the minimum calculated O content is ~5 atoms per formula unit. Subtraction of 5 from the total calculated O content provides the same relative scale as in a. (c) Plot of A^{2+} cations (mainly Ca, Fe), A^{4+} cations (U, Th), and A-site vacancies.

of hydration. Structural formulas of all three samples approach AB_2O_6 stoichiometry, typical of many altered pyrochlore group minerals (Lumpkin and Ewing 1992, 1995).

Betafite sample 210 is the least altered of the Madagascar specimens. Orange, relatively unaltered areas of the sample have the highest Ca, Na, and F contents yet observed for betafite from Madagascar. These areas contain 0.65–0.83 Ca, 0.13–0.25 Na, and 0.07–0.14 F atoms per formula unit and <2 wt% H_2O (by difference). The structural formula of the least altered material contains <0.4 A-site vacancies and <0.5 Y-site vacancies. Moderately altered areas contain 0.18–0.35 Ca, <0.01 Na, and 0.00–0.08 F atoms per formula unit. H_2O content is estimated at 8–10 wt%. The structural formulas of partially altered material have approximately 1.1 A-site, 1.0 Y-site, and 0.1 X-site vacancies. The most heavily altered areas contain only 0.00–0.08 Ca, <0.01 Na, and 0.00–0.06 F atoms per formula unit and 8–15 wt% H_2O (by difference). Corresponding structural formulas have approximately 1.3 A-site, 1.0 Y-site, and 0.3 X-site vacancies. Changes in minor elements attending alteration include loss of Mn and incorporation of minor amounts of Al, Mg, Fe, Sr, Ba, and K. The amounts of Ba and K increase most rapidly when the number of A-site vacancies exceeds 1.2 atoms per formula unit. In contrast, the amount of Sr peaks at an A-site vacancy level of 0.9–1.1 atoms per formula unit and then decreases with further alteration, similar to the behavior observed in members of the pyrochlore subgroup (Lumpkin and Ewing 1995, Fig. 6).

Figure 3 summarizes alteration effects in the betafite samples (083, 204, 205 core, 210) that have not experienced significant recrystallization or major element redistribution. In general, secondary alteration involves loss of F, Na, Ca, and O, driving the altered betafite compositions toward the A^{2+} cation-vacancy join and the A-site vacancy corner of Figure 3a. Similar trends are shown for the anions and X + Y anion vacancies in Figure 3b. Increased hydration is typical of this stage of alteration, but the U and Th contents remain relatively constant (Fig. 3c). On the basis of a hypothetical end-member betafite having ideal $A_2B_2X_6Y$ stoichiometry, this stage of secondary alteration can be modeled by the reaction

$$2.5H^+ + H_2O + (CaNa_{0.5}U_{0.5}NbTiO_{6.5}F_{0.5})_{bss} = (U_{0.5}NbTiO_{5.5}\cdot 2H_2O)_{bss} + Ca^{2+} + 0.5Na^+ + 0.5HF \quad (1)$$

where the subscript bss is used to indicate a betafite solid solution. Reaction 1 is similar to previous hydration reactions written for the microlite and pyrochlore subgroups (e.g., Lumpkin and Ewing 1995, Reaction 10) and should proceed to the right under conditions of low temperature, low pH, low $a_{Ca^{2+}}$, low a_{Na^+}, and low a_{HF} in the fluid phase.

Specimen 205 provides a good example of the effects of extreme secondary alteration on members of the betafite subgroup. The core of the sample is relatively homogeneous and contains 0.16–0.22 Ca, <0.01 Na, and 0.00–0.04 F atoms per formula unit and 9–14 wt% H_2O (by difference), similar to the moderately altered areas of sample 210. Microprobe analyses of the intermediate zone (Table 4, analyses 1–5) indicate major element redistribution into several compositionally distinct "phases," which exhibit an overall loss of Ca (<0.02 Ca atoms per formula unit) and entry of significant amounts of Al (0.06–0.25 Al atoms per formula unit). Average microprobe analyses of crystalline phases and residual metamict betafite in the rim of the sample are given in Table 4 (analyses 6–9). The average analysis of rutile corresponds to the formula $Ti_{0.71}Nb_{0.13}Ta_{0.02}Fe_{0.14}O_2$. Individual analyses show a good positive correlation between Nb + Ta and Fe and a negative correlation between these elements and Ti, indicating that charge balance is maintained by the substitution $2Ti \leftrightarrow (Nb,Ta) + Fe^{3+}$. The formula of uranpyrochlore was calculated on the basis of 2.00 B-site cations assuming that Al occupies the B site, all Fe is present as Fe^{3+} at the B site, and all U is present as U^{6+}. The simplified formula of uranpyrochlore is $(U_{0.28}A_{0.09})_{0.37}(Nb_{1.42}Ti_{0.37}B_{0.21})_2O_{5.63}$, where A = Pb, Th, and REEs and B = Al, Fe, and Ta. Similar assumptions were made in the calculation of the formula of liandratite, including assignment of the small amounts of Al and Fe to the Nb site. The simplified formula of liandratite is $(U_{1.16}M_{0.28})_{1.44}(Nb_{1.14}Ti_{0.49}N_{0.28})_{1.91}O_8$, where M = K, Pb, Ba, Ca, REEs, and Th and N = Fe, Al, and Ta. The Nb-site total is reasonably close to 2.00, but the U-site total is significantly greatly than 1.00. In addition to excess U, there are substantial amounts of large cations, indicating that the chemistry is more complicated than reported in the original description of the mineral (Mücke and Strunz 1978; however, minor amounts of Al, K, Ca, and Mn were found in the related phase petscheckite, $UFeNb_2O_8$). The additional amounts of U and large cations in the

TABLE 4. Average electron microprobe analyses of betafite sample 205

	Intermediate zone phases					Rim phases				Zone averages		
	1	2	3	4	5	6	7	8	9	10	11	12
Nb_2O_5	33.0	37.0	34.1	47.6	36.1	25.2	19.2	52.6	42.0	30.2	37.9	37.6
Ta_2O_5	2.40	2.69	6.02	5.47	4.76	2.37	5.64	3.94	5.25	3.17	4.04	3.84
TiO_2	22.6	41.2	12.1	13.2	12.3	6.48	62.3	8.13	17.6	18.0	21.7	21.5
ZrO_2	0.12	0.03	2.11	0.02	0.09	0.10	0.00	0.12	0.11	0.09	0.20	0.12
ThO_2	1.22	1.58	3.16	2.70	3.05	1.19	0.00	2.08	4.26	1.45	2.30	2.18
UO_2	29.3	5.47	16.9	14.0	26.1	51.8	0.00	21.7	14.0	27.1	18.8	21.0
Al_2O_3	2.18	2.56	2.89	1.44	1.07	0.79	0.00	1.15	1.21	0.09	1.91	0.95
Y_2O_3	0.09	0.11	0.00	0.00	0.19	0.18	0.00	0.31	0.26	0.23	0.11	0.21
Ln_2O_3	0.18	0.12	0.49	0.38	0.37	0.87	0.00	0.19	0.21	0.39	0.32	0.30
MgO	0.02	0.01	0.02	0.00	0.02	0.02	0.00	0.01	0.00	0.10	0.02	0.01
CaO	0.20	0.04	0.08	0.00	0.05	0.26	0.00	0.10	0.13	2.56	0.09	0.13
MnO	0.03	0.02	0.00	0.04	0.00	0.14	0.00	0.09	0.02	0.22	0.03	0.08
FeO	2.16	4.05	1.49	0.88	0.66	1.40	11.8	1.49	1.77	2.20	1.88	3.64
BaO	0.48	0.07	0.19	0.09	0.40	0.89	0.00	0.21	0.08	0.20	0.32	0.36
PbO	2.16	1.59	15.5	3.37	2.65	2.10	0.00	3.01	2.87	1.90	3.10	2.21
Na_2O	0.08	0.02	0.00	0.00	0.05	0.05	0.00	0.01	0.00	0.00	0.03	0.02
K_2O	0.07	0.02	0.09	0.10	0.14	0.70	0.00	0.06	0.09	0.05	0.08	0.26
F	0.09	0.08	0.10	0.11	0.06	0.27	0.00	0.05	0.01	0.04	0.08	0.13
Sum	96.38	96.66	95.24	89.40	88.06	94.77	98.94	95.25	89.97	87.99	92.91	94.54
O ≡ F	−0.04	−0.03	−0.04	−0.05	−0.03	−0.11	−0.00	−0.02	−0.00	−0.02	−0.03	−0.05
Total	96.34	96.63	95.20	89.35	88.03	94.66	98.94	95.23	89.97	87.97	92.88	94.49

Note: Analyses 1–5 = metamict and poorly crystalline phases showing major element redistribution, 6 = liandratite, 7 = rutile, 8 = uranpyrochlore, 9 = residual metamict phase, 10 = average core, 11 = average intermediate zone, 12 = average rim. On average, Sr was near or below detection limits and is not reported.

structure must be charge balanced by Ti, Al, and Fe at the Nb site (see below).

Alteration of sample 205 is shown graphically using a U-Nb-Ti triangular diagram (Fig. 4a). Analyses of the core cluster near a point representing a betafite composition of $U_{0.5}NbTiO_{5.5}$. Major element redistribution within the intermediate zone is evident from compositions that plot away from the core and closer to the Nb and Ti vertices. The data also indicate overall loss of U from the intermediate zone. Compositions of crystalline phases in the rim show scatter but still define a three-phase triangle that encloses all other data points. Note that the liandratite data points in Figure 4a tend to lie along the join between UNb_2O_8 and the hypothetical end-member $U_{1.33}Ti_2O_8$ (see Fig. 4b), indicating that some of the compositional variation is accounted for by the substitution $6Nb \leftrightarrow 6Ti + U^{6+}$. Idealized phase relations for the U-Nb-Ti-O system are depicted in Figure 4b. Under conditions of weathering or low-temperature hydrothermal alteration, betafite of decreasing bulk U content can break down to liandratite + rutile, liandratite + rutile + uranpyrochlore, or rutile + uranpyrochlore. Reactions for the three idealized betafite compositions shown in Figure 4b can be written as follows using the inferred H_2O contents as a guide:

$$2(U_{0.5}NbTiO_{5.5}\cdot 2H_2O)_{bss} = UNb_2O_8 + 2TiO_2 + 3H_2O + 2H^+ + 2e^- \quad (2)$$

$$4(U_{0.375}NbTiO_{5.25}\cdot 2H_2O)_{bss} = UNb_2O_8 + (U_{0.5}Nb_2O_{6.5}\cdot H_2O)_{pss} + 4TiO_2 + 5.5H_2O + 3H^+ + 3e^- \quad (3)$$

$$2(U_{0.25}NbTiO_5\cdot 2H_2O)_{bss} = (U_{0.5}Nb_2O_{6.5}\cdot H_2O)_{pss} + 2TiO_2 + 2.5H_2O + H^+ + e^- \quad (4)$$

where the subscript pss refers to pyrochlore solid solution. Reactions 2–4 all involve dehydration, and in each case the assemblages on the right are favored by relatively high pH, high pe, or both in the fluid phase.

Changes in bulk composition attending alteration were evaluated from the average composition of each zone of sample 205. For the core, an average of the available electron microprobe analyses was used. Average compositions of the intermediate zone and rim were estimated from the average compositions of each phase together with the volume fractions determined by point counting with the use of SEM-EDS and optical microscopy, respectively. Results given in Table 4 (analyses 10–12) are consistent with the loss of approximately 20–25% of the U originally present in the intermediate zone and rim, in general agreement with the data shown in Figure 4a. The average zone compositions also suggest that the overall level of hydration decreases from the core outward, in agreement with Reactions 2–4.

Geochemical alteration of betafite 205 can be considered as a three-step process. First, the entire crystal was subject to leaching of Na, F, and Ca according to Reaction 1. Second, U was lost from the intermediate zone and rim by a reaction of the form

$$8(U_{0.5}NbTiO_{5.5}\cdot 2H_2O)_{bss} = 8(U_{0.375}NbTiO_{5.25}\cdot 2H_2O)_{bss} + UO_2^{2+} + 2e^- \quad (5)$$

where we assumed that U is present in the fluid phase as the uranyl group UO_2^{2+} for illustrative purposes only. The actual speciation of U in solution is a complex function of temperature, pH, and composition of the fluid phase

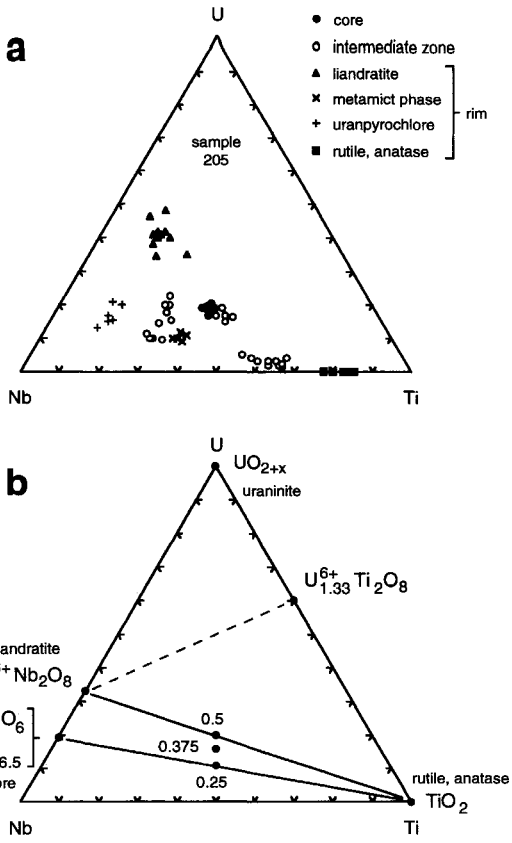

FIGURE 4. U-Nb-Ti plots (atom ratios) showing stage 2 secondary alteration of metamict betafite sample 205. (**a**) Observed relationships for the core, intermediate zone, and recrystallized rim. (**b**) Idealized phase relations. Bulk U contents of 0.25, 0.375, and 0.5 atoms per formula unit are plotted as reference points.

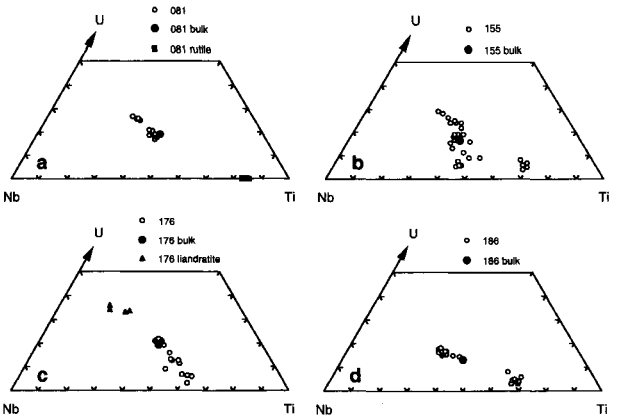

FIGURE 5. U-Nb-Ti plots (atom ratios) showing stage 2 secondary alteration and estimated bulk compositions of metamict betafite samples 081 (**a**), 155 (**b**), 176 (**c**), and 186 (**d**).

(e.g., Langmuir 1978; Brookins 1984; Johnson and Shoesmith 1988). Third, extensive recrystallization of the rim to an assemblage of liandratite + rutile + uranpyrochlore then proceeded according to Reaction 3.

Four additional betafite samples (081, 155, 176, 186) show alteration effects similar to the intermediate zone of sample 205, although the extent of recrystallization is less dramatic. For these samples, we estimated the bulk compositions from SEM-EDS area scans. Varying degrees of major element redistribution are seen on plots of the analyses on U-Nb-Ti diagrams (Fig. 5). Sample 081 contains 0.10–0.15 Ca, 0.00–0.02 Na, 0.00–0.02 F, and 0.00–0.02 Al atoms per formula unit and 9–11 wt% H_2O (by difference). The specimen shows minor skewing of data points away from the estimated bulk composition toward the U-Nb join along with minor amounts of a crystalline rutile-like phase (Fig. 5a). The average composition of this phase is $Ti_{0.72}Nb_{0.13}Ta_{0.03}Fe_{0.12}O_2$, nearly identical in composition to rutile in the rim of sample 205.

Betafite sample 155 contains 0.00–0.04 Ca, <0.01 Na, 0.00–0.02 F, and 0.00–0.04 Al atoms per formula unit and 2–11 wt% H_2O (by difference). Compositions scatter around the estimated bulk composition toward the U-Nb and Nb-Ti joins, with a separate cluster of points approximately halfway toward the Ti vertex of Figure 5b. As noted in the sample description (see Fig. 2b), veinlets of U- and Ti-rich material occur in the sample together with euxenite and hematite. Analyses of the U-rich and Ti-rich veinlets plot at the extremes shown in Figure 5b and represent the most advanced stage of major element redistribution in the sample. Patchy areas and veinlets of euxenite and hematite may represent earlier hydrothermal alteration of the betafite. Electron microprobe analyses of euxenite give an average chemical formula of $(REE_{0.62}A_{0.41})_{1.03}(Nb_{0.96}Ti_{0.95}Ta_{0.07})_{1.98}O_6$, where A = Ca, U, Th, Fe, Mn, and Pb. In general, the composition is typical of the euxenite mineral group (Ewing 1975; Černý and Ercit 1989). Interestingly, the B-site cation content is nearly identical to that of the host betafite and is consistent with replacement by A-site cation exchange. The hematite contains very few elemental impurities and ranges in composition from $Fe_{1.99}Al_{0.01}O_3$ to $Fe_{1.78}Ti_{0.20}Mn_{0.02}O_3$.

Sample 176 contains 0.00–0.03 Ca, <0.01 Na, 0.00–0.09 F, and 0.10–0.14 Al atoms per formula unit but only 1–6 wt% H_2O (by difference). Figure 5c shows a small cluster of data points near the estimated bulk composition, an almost continuous scatter of data points toward the Nb-Ti join, and a group of data points toward the U-Nb join identified as liandratite. The significant major element of redistribution away from the original bulk composition of the sample towards phase compositions with a lower level of hydration may explain the unusually low estimated H_2O content of betafite 176. The average composition of liandratite is $(U_{1.00}M_{0.27})_{1.27}(Nb_{1.30}Ti_{0.54}N_{0.19})_{2.03}O_8$, where M = K, Pb, Ba, Ca, REEs, and Th and N = Al, Ta, and Fe. Although the U content is lower than that of liandratite in the rim of sample 205, the composition is otherwise similar and confirms the presence of significant amounts of K, Ca, Ba, and REEs in the mineral. In this case, the major charge-balancing substitutions are Nb ↔ Ti + K, 2Nb ↔

2Ti + (Ca, Ba, Pb), and 3Nb ↔ 3Ti + REE. Additional charge balance is provided by small amounts of Al and Fe at the Nb site.

Specimen 186 also displays two groups of data points, one lying near the estimated bulk composition with minor scatter toward the U-Nb join and a separate cluster halfway toward the Ti vertex of Figure 5d. Contents of 0.06–0.35 Ca, <0.01 Na, 0.01–0.11 F, 0.01–0.12 Al, and 0.01–0.16 Pb atoms per formula unit and approximately 8–16 wt% H_2O (by difference) are typical of the specimen. In addition to the observed chemical variability and major element segregation, veinlets of goethite occur as an alteration product of this sample. The average composition of the goethite is $Fe_{0.94}Ti_{0.02}Mg_{0.01}Al_{0.01}Mn_{0.01}Nb_{0.01}OOH$.

Effect of alteration on annealing products

Annealing of members of the betafite subgroup in an inert atmosphere (N_2) at 1000 °C commonly leads to the formation of rutile, liandratite, and pyrochlore. Heating products appear to be controlled in part by the U content (see Fig. 4b) according to the phase relations described above for the group of samples with low Ca content. For example, sample 176 has an average U + Th content close to 0.5 atoms per formula unit and recrystallizes primarily to liandratite + rutile. Betafite samples 081, 155, 205, and 210 have lower average U + Th contents lying between 0.35 and 0.45 atoms per formula unit, and all four anneal to the three-phase assemblage consisting of liandratite + rutile + uranpyrochlore. Specimen 186 has an even lower bulk U + Th content of approximately 0.3 atoms per formula unit and anneals mainly to uranpyrochlore + rutile. Results for these six samples are generally consistent with the idealized phase relations depicted in Figure 4b.

Three other betafite samples (083, 178, 204) have moderate U + Th contents (0.38–0.43 atoms per formula unit), placing them in the three-phase region of Figure 4b, but anneal mainly to uranpyrochlore with minor to moderate amounts of rutile. The deciding factor for this group of samples appears to be the relatively high Ca content of 0.39–0.65 atoms per formula unit (5.2–9.0 wt% CaO). With increasing Ca content in the system Ca-U-Nb-Ti-O, the bulk compositions of these samples must intersect the two-phase field of uranpyrochlore + rutile. For bulk Ca contents above those represented by this group of samples, the bulk composition should eventually lie within the stability field of betafite solid solution, resulting in minimal amounts of rutile being formed on annealing.

U-Pb systematics

Metamict betafite samples from Madagascar have an age of approximately 550 Ma (Mücke and Strunz 1978) and have low Th contents of 0.00–0.04 atoms per formula unit. Data in Figure 6a show that the U and Pb contents of the least altered areas cluster near the 550 Ma reference line with a maximum Pb loss of ~30% (assuming a low initial Pb content). The data points representing

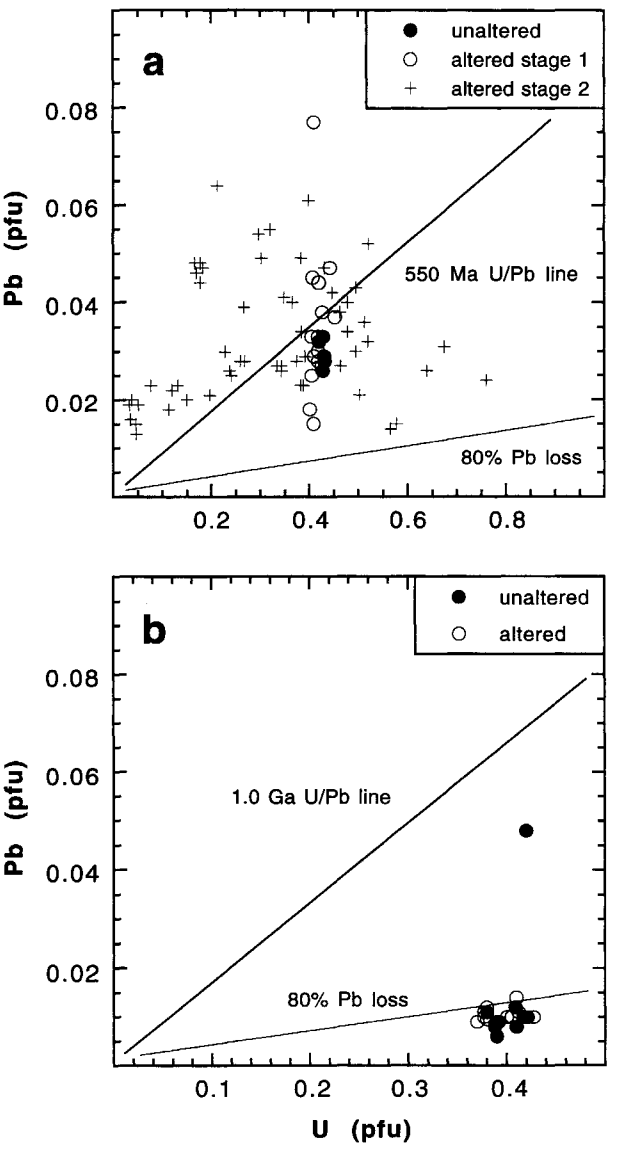

FIGURE 6. U-Pb systematics (atoms per formula unit) of unaltered and altered betafite samples. (a) Results for 550 m.y. old Madagascar samples 081, 155, 176, 205, and 210. (b) Results for 1000 m.y. old Canadian samples 083 and 204. A single high Pb data point may have resulted from a small grain of galena located within the excitation volume of the electron probe.

secondary alteration prior to significant major element segregation (alteration stage 1) exhibit additional vertical scatter above and below the unaltered data points. In contrast, data representing areas of major element segregation (alteration stage 2) display a large amount of scatter consistent with the internal mobility of both U and Pb during this stage of alteration. Gross trends in the data indicate that specific areas within the betafite samples were enriched in Pb and depleted in U, depleted in both U and Pb, or enriched in U and depleted in Pb relative to a point on the 550 Ma reference line above

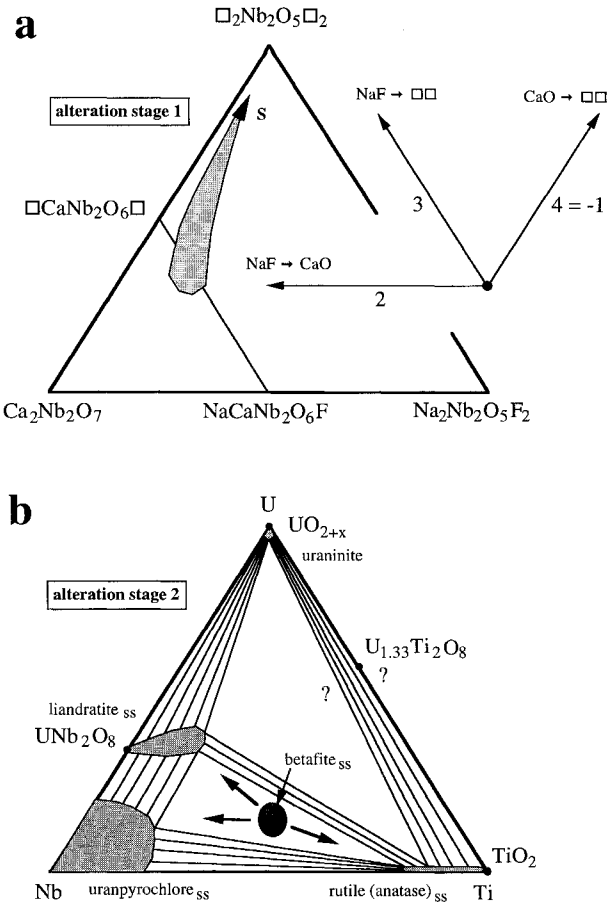

FIGURE 7. Schematic summary of secondary alteration effects in metamict betafite. (**a**) Stage 1 involves chemical alteration and loss of Na, Ca, F, and O. Alteration paths (S) initially fall between vectors 3 and 4, rotating toward vector 4 with increasing alteration. (**b**) Stage 2 involves major element mobility and recrystallization, beginning when Ca content falls below 0.2–0.3 atoms per formula unit (~2.5 wt% CaO). Solid-solution, two-phase, and three-phase fields are approximations for near-surface and weathering environments.

the unaltered compositions (~0.4 U and 0.035 Pb atoms per formula unit). Stage 2 analyses contain an average of 0.32 U and 0.04 Pb atoms per formula unit, suggesting that most of the U and Pb has remained within the immediate confines of the betafite samples.

Betafite samples from Grenville rocks near Bancroft, Ontario, Canada, have an age of approximately 1 Ga, typically contain <0.01 Th atoms per formula unit, and are completely metamict. The U and Pb contents plotted in Figure 6b indicate Pb loss of up to 80–90% from both altered and unaltered areas of the samples, consistent with a model of long-term Pb loss proposed previously for the microlite and pyrochlore subgroups (Lumpkin and Ewing 1992, 1995). However, in these samples a portion of the radiogenic Pb lost by diffusion may have been retained within precipitates of galena, which formed in voids and microfractures in the presence of an S-bearing fluid. Similar results have recently been reported for samples of metamict zirconolite from the Phalaborwa carbonatite complex (age ~2.5 Ga), South Africa (Gieré et al. 1994; Lumpkin et al. 1994).

DISCUSSION

Chemical effects of alteration

The chemical changes that accompany secondary alteration of betafite can be described in two stages as illustrated in Figure 7. In stage 1 (Fig. 7a), the alteration mainly involves mobility of A-site cations, Y-site anions, and X-site anions, following a path between vectors 3 ($^{A}Na^{Y}F \rightarrow {}^{A}\square^{Y}\square$) and 4 ($^{A}Ca^{Y}O \rightarrow {}^{A}\square^{Y}\square$ and $^{A}Ca^{X}O \rightarrow {}^{A}\square^{X}\square$), essentially the same path found previously for the microlite and pyrochlore subgroups (cf. Lumpkin and Ewing 1992, Fig. 8; Lumpkin and Ewing 1995, Fig. 9). Under these conditions the U and Th contents remain relatively constant down to a Ca content of approximately 0.2–0.3 atoms per formula unit (~2.5–3.5 wt% CaO). Betafite from Madagascar generally exhibits loss of Mn along with Ca, Na, and F, compensated in part by increasing amounts of Fe, Sr, Ba, and K. The amount of Sr tends to increase at a faster rate than Ba or K, peaking at an intermediate level of Ca loss, then decreasing. Ba and K usually reach peak concentrations after most of the Ca has been removed. In general, the leaching and cation-exchange effects follow the valence and ionic radius criteria proposed for the pyrochlore subgroup (Lumpkin and Ewing 1995). The ability to apply these criteria to radiation-damaged samples emphasizes the importance of the B_2X_6 framework of the pyrochlore structure. The chemical results of this study are entirely consistent with a model of the metamict state in pyrochlore in which the B_2X_6 framework essentially remains intact but loses periodicity beyond the second coordination sphere (Lumpkin and Ewing 1988).

The retention of U and Th during stage 1 is further supported by the measured activity ratios of ^{238}U, ^{234}U, ^{230}Th, ^{232}Th, and ^{228}Th in sample 210, which are all unity, indicating that the sample has remained a closed system isotopically for the last ~10^6 yr (Lumpkin et al. 1988, Table III). Although the mobility and extensive loss of radiogenic Pb in the Canadian samples can be explained by volume diffusion over long periods of time (Nicolaysen 1957; Tilton 1960), the process may be aided by extensive radiation damage, volume expansion, and microfracturing, resulting in an effective reduction in grain size and providing numerous pathways for hydrothermal and low-temperature fluids (Wayne and Sinha 1988; Gieré et al. 1994; Lumpkin et al. 1994).

Stage 2 commences when Ca content drops below 0.2–0.3 atoms per formula unit, resulting in defect betafite compositions lying within the stability field of rutile, liandratite, and uranpyrochlore, thus promoting major element mobility and incipient recrystallization (Fig. 7b). This stage of secondary alteration is accompanied by ma-

jor increases in the amount of Al, a relatively small cation not normally found in unaltered betafite above the 0.1–0.2 wt% level as Al_2O_3. Loss of up to 20–30% of the original amount of U may occur at this stage, but a large proportion of the U lost from betafite may be retained nearby in the form of secondary phases (e.g., as U^{6+} in liandratite) or even adsorbed on secondary iron oxides and clay minerals (Ivanovich 1994). The new phase assemblage formed by recrystallization of chemically altered, metamict betafite is controlled mainly by the bulk U content. With decreasing bulk U content, the predicted phase assemblages are liandratite + rutile, liandratite + rutile + uranpyrochlore, and rutile + uranpyrochlore. These relationships were confirmed by heating experiments in an inert atmosphere. Of the TiO_2 polymorphs, both anatase and rutile were identified, typical of alteration at relatively low temperatures.

Conditions of alteration

Most of the betafite samples investigated here crystallized under the magmatic conditions characteristic of geochemically primitive granitic pegmatites (~550–650 °C, 2–5 kbar) and carbonatites. (Depending on composition and volatile content, final emplacement occurred at ~450–690 °C and <2 kbar; see review of Heinrich 1980. Fluid-inclusion studies indicate initial crystallization at ≥625 °C and ≥4 kbar in some carbonatites; see Andersen 1986; Morogan and Lindblom 1995.) Furthermore, the betafite samples may have experienced late-stage hydrothermal activity to temperatures as low as 350 °C in granitic pegmatites and 200 °C in carbonatites (see Lumpkin and Ewing 1992, 1995, and references therein). However, unlike for the microlite and pyrochlore subgroups, there is little evidence to suggest that any of the betafite samples were altered under these conditions. The observed secondary alteration of betafite is undoubtedly promoted by extensive radiation damage, volume expansion, and microfracturing and is so pervasive that evidence of prior alteration is likely to be erased.

Secondary alteration of betafite appears to be caused by relatively low temperature and relatively acidic groundwater having low activities of Na, Ca, and F. Although the precise conditions of alteration are not known, the observed secondary phases and host-rock alteration are consistent with near-surface weathering processes resulting in increased activities of Fe, Sr, Ba, K, and Al at temperatures <100 °C. In the geothermal field of Antsirabé, Madagascar (near Betafo, the type locality of betafite), Sarazin et al. (1986) measured near surface waters with temperatures of 15–25 °C, pH of 6.2–7.4, relatively low Na, K, Ca, and Mg contents, trace amounts of K, Fe, and Al, and low total alkalinity. The reported groundwater compositions are in general agreement with the chemical effects of alteration observed in betafite, particularly for the examples of K, Fe, and Al mobility.

The occurrence of rutile (or anatase) as an alteration product of betafite is in accordance with groundwater compositions having low Ca^{2+} and dissolved silica concentrations. Nesbitt et al. (1981) determined that many natural groundwaters in host rocks ranging from basaltic to granitic in composition plot within the stability field of rutile, with a few compositions in the stability field of titanite at log $(a_{Ca^{2+}}/a^2_{H^+})$ values above ~13. Similar conclusions apply to groundwaters of the Canadian Shield at subsurface levels down to 500 m (Hayward 1988, Figs. 5 and 6). Fluid compositions and pH values determined by Sarazin et al. (1986) for the Antsirabé groundwater samples also plot mainly in the rutile stability field at log $(a_{Ca^{2+}}/a^2_{H^+})$ values of approximately 7–13 and log a_{SiO_2} values between −3 and −4 (see Fig. 3 in Nesbitt et al. 1981).

Conclusions

Studies of natural pyrochlore in general have provided a considerable amount of information bearing on aspects of the long-term performance of pyrochlore phases in titanate-based ceramic nuclear waste forms, including tailored ceramics (Harker 1988) and Synroc (Ringwood et al. 1988; Ball et al. 1989). Of the three pyrochlore subgroups, studies of natural betafite may have direct application to the titanate ceramic designed for disposal of partially reprocessed nuclear fuel elements (see Ball et al. 1989 and references therein). This waste form consists of betafite of near ideal stoichiometry ($CaUTi_2O_7$) as a major phase together with hollandite, perovskite, and uraninite. The conclusions outlined above suggest that the long-term stability of the waste form is in part governed by leaching of Ca and recrystallization of betafite to secondary phases in the U-Ti-O system.

Our studies of the geochemistry of pyrochlore (Lumpkin and Ewing 1985, 1992, 1995) demonstrate the following: (1) Microlite, pyrochlore, and betafite are subject to cation and anion exchange and leaching under conditions ranging from hydrothermal (maximum ~650 °C and 5 kbar) to near surface, weathering environments. The fluids responsible for alteration range from dense, supercritical magmatic fluids, to mixed magmatic-meteoric fluids, to groundwaters of low ionic strength. (2) To a first approximation, A-site cation mobility is limited by valence and ionic radius constraints. The least mobile A-site cations are REE^{3+}, Th^{4+}, and U^{4+}. Actinides are effectively retained by microlite, pyrochlore, and most betafite samples for geological time periods up to 1.4 b.y. (3) Extensive leaching of cations from betafite places the bulk composition in the stability field of liandratite, uranpyrochlore, and rutile (or anatase). These betafite samples are subject to major element mobility, recrystallization, and in extreme situations exhibit some U loss. (4) In addition to the prevailing *PTX* conditions, the extent of alteration is influenced by grain size, prior radiation damage and microfracturing, volume and flow rate of the hydrothermal fluid or groundwater, and total exposure time. (5) Samples from laterite horizons and other weathering environments demonstrate that the rate of ion exchange exceeds the total dissolution rate, governed primarily by the stability of the octahedral framework when occupied by Nb, Ta, and Ti. (6) In some pyrochlore group minerals

TABLE 5. Chemical definitions

Definition	Substitution scheme	Exchange operator	Additional effects
NaF-CaO exchange	$^{A}Na^{Y}F \rightarrow {}^{A}Ca^{Y}O$	$CaO(NaF)_{-1}$	±Mn, Fe, Sr
NaF leaching	$^{A}Na^{Y}F \rightarrow {}^{A}\square^{Y}\square$	$\square\square(NaF)_{-1}$	±Sr, Ba, REEs
CaO leaching	$^{A}Ca^{X,Y}O \rightarrow {}^{A}\square^{X,Y}\square$	$\square\square(CaO)_{-1}$	±K, Sr, Ba, etc.

where extensive alteration has taken place, the textural criteria become difficult to apply, indicating that alternative chemical definitions may be more appropriate. We suggest that the chemical definitions given in Table 5 be adopted (exchange operator notation after Burt 1989).

ACKNOWLEDGMENTS

Samples used in this investigation were kindly provided by Carl Francis (Harvard University), Gordon Brown (Stanford University), John S. White (Smithsonian Institution), and George Harlow (American Museum of Natural History). We thank Scott Ercit and Don Burt for constructive reviews of the manuscript. Most of this work was completed in the Electron Microbeam Analysis Facility in the Department of Earth and Planetary Sciences at the University of New Mexico, supported in part by NSF, NASA, DOE-BES (grant DE-FG03-93ER45498), and the State of New Mexico.

REFERENCES CITED

Andersen, T. (1986) Magmatic fluids in the Fen carbonatite complex, S.E. Norway: Evidence of mid-crustal fractionation from solid and fluid inclusions in apatite. Contributions to Mineralogy and Petrology, 93, 491–503.

Ball, C.J., Buykx, W.J., Dickson, F.J., Hawkins, K., Levins, D.M., Smart, R.St.C., Smith, K.L., Stevens, G.T., Watson, K.G., Weedon, D., and White, T.J. (1989) Titanate ceramics for the stabilization of partially reprocessed nuclear fuel elements. Journal of the American Ceramic Society, 72, 404–414.

Brookins, D.G. (1984) Geochemical aspects of radioactive waste disposal, 347 p. Springer-Verlag, New York.

Burt, D.M. (1989) Compositional and phase relations among rare earth element minerals. In Mineralogical Society of America Reviews in Mineralogy, 21, 259–307.

Černý, P., and Ercit, T.S. (1989) Mineralogy of niobium and tantalum: Crystal chemical relationships, paragenetic aspects and their economic implications. In P. Möller, P. Černý, and F. Saupé, Eds., Lanthanides, tantalum and niobium, p. 27–79. Springer-Verlag, Berlin.

Ewing, R.C. (1974) Spherulitic recrystallization of metamict polycrase. Science, 184, 561–562.

——— (1975) Alteration of metamict, rare-earth, AB_2O_6-type Nb-Ta-Ti oxides. Geochimica et Cosmochimica Acta, 39, 521–530.

Gieré, R., Guggenheim, R., Düggelin, M., Mathys, D., Williams, C.T., Lumpkin, G.R., Smith, K.L., Blackford, M.G., Hart, K.P., and McGlinn, P. (1994) Retention of actinides during alteration of aperiodic zirconolite. Proceedings of the 13th Conference on Electron Microscopy, p. 1269–1270. Paris, France.

Harker, A.B. (1988) Tailored ceramics. In W. Lutze and R.C. Ewing, Eds., Radioactive waste forms for the future, p. 335–392. North-Holland, Amsterdam.

Hayward, P.J. (1988) Glass-ceramics. In W. Lutze and R.C. Ewing, Eds., Radioactive waste forms for the future, p. 427–494. North-Holland, Amsterdam.

Heinrich, E.W. (1980) The geology of carbonatites, p. 186–215. Kreiger, Huntington, New York.

Hogarth, D.D. (1961) A study of pyrochlore and betafite. Canadian Mineralogist, 6, 610–633.

——— (1977) Classification and nomenclature of the pyrochlore group. American Mineralogist, 62, 403–410.

Ivanovich, M. (1994) Uranium series disequilibrium: Concepts and applications. Radiochimica Acta, 64, 81–94.

Johnson, L.H., and Shoesmith, D.W. (1988) Spent fuel. In W. Lutze and R.C. Ewing, Eds., Radioactive waste forms for the future, p. 635–698. North-Holland, Amsterdam.

Kennedy, I. (1979) Some interesting radioactive minerals from the Bancroft area, Ontario. Mineralogical Record, 10, 153–158.

Langmuir, D. (1978) Uranium-solution mineral equilibria at low temperatures with applications to sedimentary ore genesis. Geochimica et Cosmochimica Acta, 42, 547–570.

Lumpkin, G.R. (1989) Alpha-decay damage, geochemical alteration, and crystal chemistry of pyrochlore group minerals. Ph.D. dissertation, University of New Mexico, Albuquerque.

Lumpkin, G.R., and Ewing, R.C. (1985) Natural pyrochlores: Analogues for actinide host phases in radioactive waste forms. In C.M. Jantzen, J.A. Stone, and R.C. Ewing, Eds., Scientific basis for nuclear waste management VIII, Materials Research Society Symposium Proceedings, 44, 647–654. Materials Research Society, Pittsburgh, Pennsylvania.

——— (1988) Alpha-decay damage in minerals of the pyrochlore group. Physics and Chemistry of Minerals, 2, 2–20.

——— (1992) Geochemical alteration of pyrochlore group minerals: Microlite subgroup. American Mineralogist, 77, 179–188.

——— (1995) Geochemical alteration of pyrochlore group minerals: Pyrochlore subgroup. American Mineralogist, 80, 732–743.

Lumpkin, G.R., Ewing, R.C., and Eyal, Y. (1988) Preferential leaching and natural annealing of alpha-recoil tracks in metamict betafite and samarskite. Journal of Materials Research, 3, 357–368.

Lumpkin, G.R., Smith, K.L., Blackford, M.G., Hart, K.P., McGlinn, P., Gieré, R., and Williams, C.T. (1994) Prediction of the long-term performance of crystalline nuclear waste form phases from studies of mineral analogues. Proceedings of the 9th Pacific Basin Nuclear Conference, p. 879–885. Sydney, Australia.

Mazzi, F., and Munno, R. (1983) Calciobetafite (new mineral of the pyrochlore group) and related minerals from Campi Flegrei, Italy; crystal structures of polymignite and zirkelite: Comparison with pyrochlore and zirconolite. American Mineralogist, 68, 262–276.

Morogan, V., and Lindblom, S. (1995) Volatiles associated with the alkaline-carbonatite magmatism at Alnö, Sweden: A study of fluid and solid inclusions in minerals from the Långarsholmen ring complex. Contributions to Mineralogy and Petrology, 122, 262–274.

Mücke, A., and Strunz, H. (1978) Petscheckite and liandratite, two new pegmatite minerals from Madagascar. American Mineralogist, 63, 941–946.

Nesbitt, H.W., Bancroft, G.M., Fyfe, W.S., Karkhanis, S.N., Nishijima, A., and Shin, S. (1981) Thermodynamic stability and kinetics of perovskite dissolution. Nature, 289, 358–362.

Nicolaysen, L.O. (1957) Solid diffusion in radioactive minerals and the measurement of absolute age. Geochimica et Cosmochimica Acta, 11, 41–59.

Ringwood, A.E., Kesson, S.E., Reeve, K.D., Levins, D.M., and Ramm, E.J. (1988) Synroc. In W. Lutze and R.C. Ewing, Eds., Radioactive waste forms for the future, p. 233–334. North-Holland, Amsterdam.

Sarazin, G., Michard, G., Rakotonindrainy, and Pastor, L. (1986) Geochemical study of the geothermal field of Antsirabé (Madagascar). Geochemical Journal, 20, 41–50.

Tilton, G.R. (1960) Volume diffusion as a mechanism for discordant lead ages. Journal of Geophysical Research, 65, 2933–2945.

Wayne, D.M., and Sinha, A.K. (1988) Physical and chemical response of zircons to deformation. Contributions to Mineralogy and Petrology, 98, 109–121.

MANUSCRIPT RECEIVED JUNE 5, 1995
MANUSCRIPT ACCEPTED APRIL 29, 1996